Entropy generation over nonlinear thermally radiative and mixed convective nanofluid flow

Sharmistha Ghosh[1*], *Sewli* Chatterjee,[2] and *Hiranmoy* Mondal[3]

[1]Department of Basic Science and Humanities, Institute of Engineering and Management, University of Engineering and Management, Kolkata, India
[2]Department of Mathematics, THLH Mahavidyalaya (Under Burdwan University), West Bengal, India
[3]Department of Applied Mathematics, Maulana Abul Kalam Azad University of Technology, West Bengal, India

Abstract This study focuses on incompressible nanofluid flow over nonlinear stretching boundary layer with viscous dissipation and thermal radiation. The effect of thermophoresis with diffusive Brownian motion and uniform heat generation or absorption is also studied. The entropy generation analysis is performed for this model. The spectral quasi-linearisation technique is employed to determine the impact of different parameters of interest, as Nusselt and Sherwood numbers. The performance of the numerical scheme is examined through residual error analysis that reveals the robustness of the present method in rendering rapidly convergent solutions.

Keywords: Nanofluid; nonlinear stretching surface; boundary layer flow; viscous dissipation; diffusion.

1 Introduction

In the past few years, heat transfer phenomena have become more critical in diverse scientific and technical regimes. This has notable applications in electronic equipment, energy plants, maritime industries, and chemical and medical devices. It is essential to understand heat transfer and the related cooling processes to come to a decision for the design of heat exchangers, radiators with optimal shape, and many more.

In 2020, Patra, Nayak, and Misra [1] investigated MHD Falkner-Skan flow on a tangent hyperbolic nanofluid model. They considered chemical reactions, non-constant suction parameters,

activation energy, and heat generation. It was noticed that an increment in the rate of chemical reaction reduces the volume fraction of nanoparticles, whereas activation energy demonstrates an opposite tendency. Afridi, Kasim, and Khan [2] examined entropy generation considering a magnetic field that is non-uniform including the sequel of Joule heating and viscous dissipation. They solved the converted ODE by shooting method with the fourth-order Runge-Kutta technique. Shah, Kumam, and Deebani [3] studied Casson nanofluid involving electrical conduction and radiation. They observed a boost in thermal boundary layer as well as entropy with increment in radiation. In 2021, Sandhya et al. [4] examined the radiative and MHD fluid flow model taking into consideration the sequel of activation energy along with second-order velocity slip condition. In 2020, El-Zahar, Rashad, and Seddek [5] scrutinized Jeffrey MHD nanofluid with mixed convection for the repercussions of Brownian motion as well as viscous dissipation. They observed that a rise in magnetic field strength increased the Nusselt number whereas there was a decrement in skin friction. Qureshi [6] studied thermal radiation of Williamson nanofluid MHD flow. Several researchers [7-17] examined the entropy generation on various kinds of nanofluids past different surfaces and geometries. Recently, in 2024, Samantara et al. [18] presented a critical review of entropy analysis of composite nanofluids. It is observed that hybrid nanofluids exhibit maximum entropy in comparison to single nanofluids.

A magnetic field exhibits a crucial influence on momentum since Lorentz force is generated in presence of the field, which acts in opposition to velocity, and as a consequence, the fluid velocity diminishes. Many researchers [19-22] studied the behavior of magnetic fields in mass and heat transportation of nanofluid flow. Ali et al. [23] investigated the Cattaneo-Christov nanofluid model in the presence of microbes with thermal radiation. Waqas et al. [24, 25] examined bioconvective flow with

*Corresponding Author's Email: sharmisthag71@gmail.com

gyrotactic micro-organisms, while Khan et al. [26] studied bioconvection with activation energy. Al-Khaled, Khan & Khan [27] discussed the microbe's profile with chemical reactions. Usman et al. [28] examined electrically conducting nanofluid for mass and heat transfer. Arshad et al. [29] investigated the impact of inclined magnetic field on hybrid nanofluid that is chemically reactive. Recently, in 2024, magnetic nanofluids, that have highly responsive magnetic properties were examined by Xu et al. [30].

In this exploration, the authors examine the dynamics of nanofluid MHD flow over nonlinear stretching boundary layer with viscous dissipation and thermal radiation. The spectral quasi-linearisation strategy is adapted for solving the governing equations and thus determining the flow dynamics. The entropy generation analysis is also performed. The velocity, temperature, and mass transfer profiles are computed to ascertain the impact of different parameters such as residual error, Nusselt, and Sherwood numbers.

2 Mathematical Formulations

The modeled equations governing the laws of mass, momentum, energy and concentration are presented as

$$\frac{\partial u}{\partial x}+\frac{\partial v}{\partial y}=0, \tag{1}$$

$$u\frac{\partial u}{\partial x}+v\frac{\partial u}{\partial y}=\nu\frac{\partial^2 u}{\partial y^2} \tag{2}$$

$$u\frac{\partial T}{\partial x}+v\frac{\partial T}{\partial y}=\alpha_m\frac{\partial^2 T}{\partial y^2}+\tau\left[D_B\frac{\partial C}{\partial y}\frac{\partial T}{\partial y}+\left(\frac{D_T}{T_\infty}\right)\left(\frac{\partial T}{\partial y}\right)^2\right]+\frac{\mu}{\rho C_p}\left[\frac{u^2}{K}+\left(\frac{\partial u}{\partial y}\right)^2\right]-\frac{1}{\rho C_p}\frac{\partial q_r}{\partial y} \tag{3}$$

$$u\frac{\partial C}{\partial x}+v\frac{\partial C}{\partial y}=D_B\frac{\partial^2 C}{\partial y^2}+\left(\frac{D_T}{T_\infty}\right)\frac{\partial^2 T}{\partial y^2} \tag{4}$$

The associated boundary conditions are

$$u=ax^n,\quad v=0,\quad T=T_w,\quad C=C_w\quad \text{at}\quad y=0$$

$$u=v=0,\quad T=T_\infty\quad C=C_\infty\quad \text{as}\quad y\to\infty \tag{5}$$

Now, u, v denote velocity components along x, y co-ordinate directions, T represents the fluid temperature, C is solute concentration, ρ_f stands for the base fluid density, D_T is the thermophoresis diffusion coefficient, D_B is the Brownian diffusion coefficient, $(\rho C)_f$ is the heat capacitance of the base fluid, $(\rho C)_p$ is that of the nanoparticles, $\tau=(\rho C)_p/(\rho C)_f$, α_m denotes thermal diffusivity, μ represents dynamic viscosity, ν stands for kinematic viscosity, k denotes thermal conductivity, K represents permeability of the porous medium.

3 Similarity Transformation

To solve the governing equations, a similarity transformation is applied as follows:

$$\eta=y\sqrt{\frac{a(n+1)}{2\nu}}x^{\frac{n-1}{2}},u=ax^n f'(\eta),v=-\sqrt{\frac{a(n+1)\nu}{2}}x^{\frac{n-1}{2}}\left[f(\eta)+\frac{n-1}{n+1}\eta f'(\eta)\right],$$

$$\theta(\eta)=\frac{T-T_\infty}{T_w-T_\infty},\phi(\eta)=\frac{C-C_\infty}{C_w-C_\infty} \tag{6}$$

The constitutive equations (1) - (4) together with the boundary constraints (5) now take the form

$$f'''+ff''-\left(\frac{2n}{n+1}\right)f'^2=0 \tag{7}$$

$$[1+Nr\{1+(\theta_w-1)\theta\}^3]\theta''+3Nr(\theta_w-1)\{1+(\theta_w-1)\theta\}^2\theta'^2$$

$$+Pr[f\theta' + Nb\theta'\phi' + Nt\theta'^2 + \frac{2}{n+1}Eck_1f'^2 + Ecf^{"2}] = 0 \tag{8}$$

$$\phi^{"} + 0.5Lef\phi' + \frac{Nt}{Nb}\theta^{"} = 0 \tag{9}$$

and

$$f = S,\ f' = \lambda,\ \theta = 1,\ \phi = 1 \quad at \quad \eta = 0,$$

$$f' = 0,\ \theta = 0,\ \phi = 0 \quad as \quad \eta \to \infty. \tag{10}$$

Here, S represents suction or injection parameter, λ denotes stretching or shrinking parameter, $Pr = \frac{\nu}{\alpha}$ stands for Prandtl number, $Ec = \frac{u_w^2}{(C_p)_f(T_w - T_\infty)}$ denotes Eckert number, $Le = \frac{\nu}{D_B}$ is Lewis number, $Nr = \frac{16\sigma^* T_\infty^3}{3K^* k}$ represents thermal radiation parameter, $Nb = \frac{(\rho C)_p D_B(C_w - C_\infty)}{(\rho C)_f \nu}$ stands for Brownian motion parameter, $Nt = \frac{(\rho C)_p D_T(T_w - T_\infty)}{(\rho C)_f \nu T_\infty}$ denotes thermophoresis parameter, $k_1 = \frac{\nu}{ka}$ stands for the porous parameter.

The local Nusselt and Sherwood numbers are given by

$$Nu_x = \frac{xq_w}{k(T_w - T_\infty)}, Sh_x = \frac{xq_m}{D_B(C_w - C_\infty)}. \tag{11}$$

Here, q_w, q_m denote heat and mass fluxes at the wall.

The dimensionless Nusselt and Sherwood numbers are then given by the following expressions:

$$\sqrt{\frac{2\nu}{a}}Nu_x = -\sqrt{n+1}x^{\frac{n+1}{2}}\theta'(0) \tag{12}$$

$$\sqrt{\frac{2\nu}{a}}Sh_x = -\sqrt{n+1}x^{\frac{n+1}{2}}\phi'(0) \tag{13}$$

4 Entropy Generation

The exploration of generation of entropy for a system is very crucial to control irreversibility of energy in that system. This study focuses on reduction of entropy by supervising the amount of different key parameters. The volumetric rate of entropy of the current investigation can be modeled mathematically in the following fashion:

$$E_{gen} = \frac{k_f}{T_\infty^2}\left(\left(\frac{\partial T}{\partial y}\right)^2 + \frac{16\sigma^* T^3}{3k^* k_f}\left(\frac{\partial T}{\partial y}\right)^2\right) + \frac{RD}{T_\infty}\left(\frac{\partial T}{\partial y}\frac{\partial C}{\partial y}\right) + \frac{RD}{C_\infty}\left(\frac{\partial C}{\partial y}\right)^2. \tag{14}$$

Also, the characteristic rate of entropy generation is drafted as

$$E_0 = \frac{k_f(\Delta T)^2}{x^2 T_\infty^2}. \tag{15}$$

Then, the entropy generation number is defined as

$$N_G = \frac{E_{gen}}{E_0} = Re\{1 + Nr(1 + \chi\theta)^3\}\theta'^2 + \frac{Re\Sigma}{\chi^2}\phi'^2 + \frac{Re\Sigma}{\chi}\theta'\phi' \tag{16}$$

where $Re = \frac{u_w(x)x}{\nu}$ denotes the Reynolds number, $\Sigma = \frac{C_\infty RD}{k_f}$, $\chi = (\theta_w - 1)$.

Br represents the dimensionless Brinkman number related to heat conduction through the wall to the fluid and is given by

$$Br = \frac{\mu u_w^2(x)}{k_f \Delta T}, \Delta T = T_w - T_\infty. \tag{17}$$

Further,

$$N_1 = Re\{1 + Nr(1 + \chi\theta)^3\}\theta'^2,\ N_2 = \frac{Re\Sigma}{\chi^2}\phi'^2 + \frac{Re\Sigma}{\chi}\theta'\phi' \tag{18}$$

and the Bejan number is written as,

$$Be = \frac{N_1}{N_G} = \frac{1}{1+\Phi}, \tag{19}$$

where N_1 is entropy generation by virtue of heat transfer, N_2 is that due to diffusive and magnetic field and $\Phi = \frac{N_2}{N_1}$ represents the irreversibility ratio.

5 Solution Methodology

The similarity transformation technique remodels the governing equations into nonlinear ordinary differential equations (7) - (9). Since these nonlinear ODEs cannot be solved analytically, the spectral quasi-linearisation methodology is then employed to solve these equations along with the boundary conditions (10). Firstly, a quasi-linearisation approach based on Newton's method is applied to linearise the equations. The spectral method is then employed to solve the linearised equations. The main objective is to discretise the domain and then interpolate the data using a global approach. In the next section, the procedure is described in detail.

6 Numerical Scheme

The underlying philosophy of the quasi-linearisation approach uses the well-known Newton-Raphson method. On applying this technique to the equations (7)–(10), we derive the following iterative scheme:

$$p_{0,r} f'''_{r+1} + p_{1,r} f''_{r+1} + p_{2,r} f'_{r+1} + p_{3,r} f_{r+1} = R_f, \tag{20}$$
$$q_{0,r} \theta''_{r+1} + q_{1,r} \theta'_{r+1} + q_{2,r} f_{r+1} + q_{3,r} f'_{r+1} + q_{4,r} f''_{r+1} + q_{5,r} \phi'_{r+1} = R_\theta, \tag{21}$$
$$\gamma_{0,r} \phi''_{r+1} + \gamma_{1,r} \phi'_{r+1} + \gamma_{2,r} f_{r+1} + \gamma_{3,r} \theta''_{r+1} = R_\phi, \tag{22}$$

subject to

$$f_{r+1}(0) = s, f'_{r+1}(0) = \lambda, \theta_{r+1}(0) = 1, \phi_{r+1}(0) = 1,$$
$$f'_{r+1}(\infty) = 0, \theta_{r+1}(\infty) = 0, \phi_{r+1}(\infty) = 0. \tag{23}$$

The coefficients appearing in equations (19)–(21) are

$$p_{0,r} = 1, p_{1,r} = f_r, p_{2,r} = -(4n/(n+1)) f'_r, p_{3,r} = f''_r, \tag{24}$$
$$q_{0,r} = \frac{1+Nr}{Pr}, q_{1,r} = f_r + Nb\phi'_r + 2Nt\theta'_r, q_{2,r} = -2Ecf''_r,$$
$$q_{3,r} = (4/(n+1)) Eck1 f'_r, q_{4,r} = -\theta'_r, q_{5,r} = Nb\theta'_r, \tag{25}$$
$$\gamma_{0,r} = 1, \gamma_{1,r} = 0.5Lef_r, \gamma_{2,r} = 0.5Le\phi'_r, \gamma_{3,r} = \frac{1}{Le}\frac{Nt}{Nb} \tag{26}$$

A pseudo-spectral method due to Chebyshev is now applied for solving the system which uses the Gauss-Lobatto points

$$x_i = \cos\left(\frac{\pi i}{M}\right), \; i = 0,1,2,\dots,M \qquad -1 \le x_i \le 1. \tag{27}$$

Here, M stands for number of collocation points. The interval $[0, L]$ is transferred to $[-1,1]$ using a linear transformation approach, where L represents the boundary at infinity.

The Chebyshev differentiation matrix represents the derivatives with respect to η and is presented as

$$\frac{df_r^{(p)}}{d\eta^p}|_{\eta=\eta_j} = \sum_{k=0}^{M} D_{jk} f(\eta_k) = DF, \;\; j = 1,2,\dots,M. \tag{28}$$

Here $F = [f(\eta_0), f(\eta_1), f(\eta_2), \dots, f(\eta_M)]^T$ and $D = 2D/L$, where D denotes the differentiation matrix due to Chebyshev. The derivative of the order p is expressed as

$$F_r^{(p)} = D^p F. \tag{29}$$

By using the differentiation matrix D, spectral collocation is adapted at iteration r to approximate the derivative to obtain the following:

$$C_{1,1} f + C_{1,2} \boldsymbol{\theta} + C_{1,3} \boldsymbol{\phi} = R_f, \tag{30}$$
$$C_{1,2} f + C_{2,2} \boldsymbol{\theta} + C_{2,3} \boldsymbol{\phi} = R_\theta, \tag{31}$$
$$C_{1,3} f + C_{2,3} \boldsymbol{\theta} + C_{3,3} \boldsymbol{\phi} = R_\phi. \tag{32}$$

where $C_{i,j}$ is a diagonal matrix of order $(M+1)$, and $\boldsymbol{f}$ denotes the value of f, while $\boldsymbol{\theta}$ and $\boldsymbol{\phi}$ represent that of θ and ϕ, respectively. Next, we apply the spectral quasi-linearisation technique to equations (24)–(26); these are now displayed in matrix form as

$$\begin{bmatrix} C_{11} & C_{12} & C_{13} \\ C_{21} & C_{22} & C_{23} \\ C_{31} & C_{32} & C_{33} \end{bmatrix} \begin{bmatrix} F_{r+1} \\ \Theta_{r+1} \\ \phi_{r+1} \end{bmatrix} = \begin{bmatrix} R_f \\ R_\theta \\ R_\phi \end{bmatrix}. \tag{33}$$

7 Results and Discussion

We now discuss and analyze the results acquired through the present investigation. Firstly, error analysis is performed to test the efficacy and reliability of the current method.

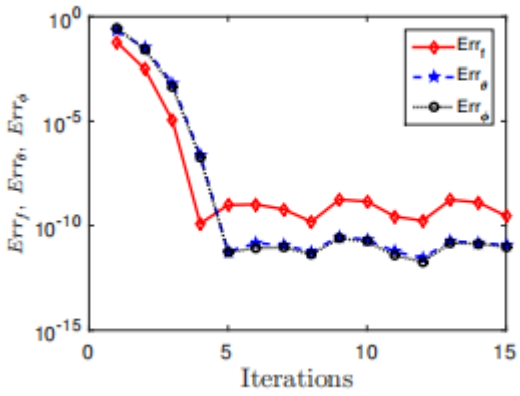

Fig. 1: Over-all error in velocity, temperature, and concentration profiles

The error profiles in calculation of velocity, temperature, and concentration functions are presented in figure 1. One may note that in just five iterations, the error diminishes to the order of 10^{-8} or less for each of the functions. This confirms that the numerical scheme is convergent as well as stable.

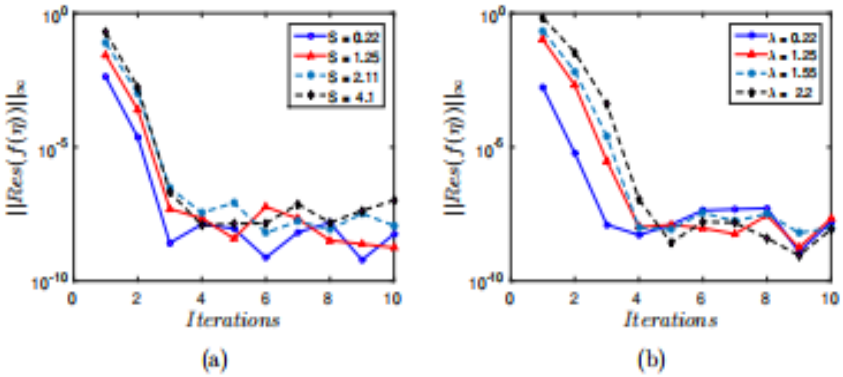

Fig. 2: Residual error in velocity function at different values of S and λ

The residual error in computation of velocity profile at varied values of the suction and stretching parameters S and λ are shown in figures 2(a), 2(b). We may again observe that the current numerical scheme is quite accurate with reasonably higher rate of convergence. Figure 2(a) depicts that the residual error in velocity function drops to the order of 10^{-7} or less in just three iterations for different values of S and stability is attained. Figure 2(b) shows that the error diminishes to similar order in four iterations with variations in λ.

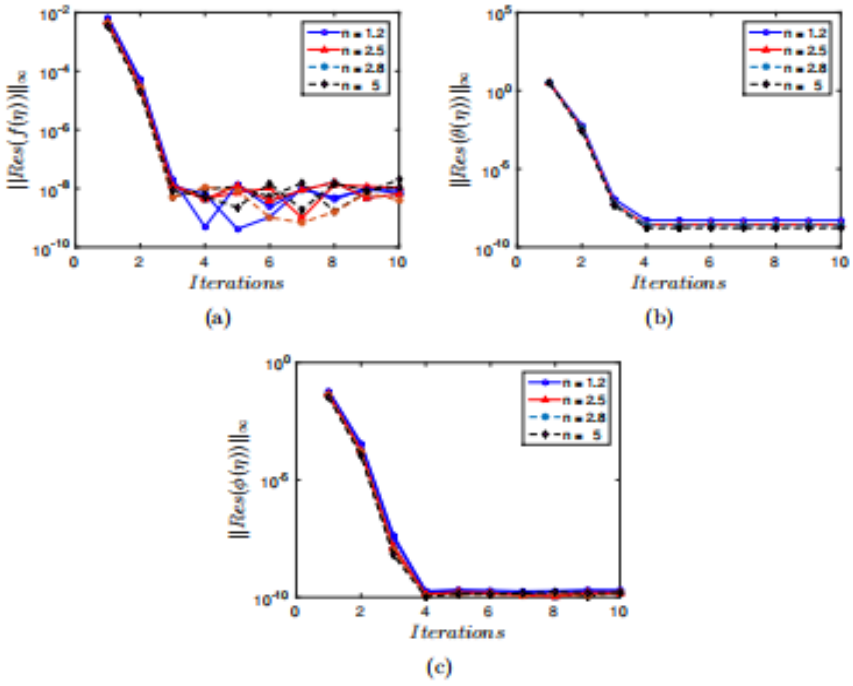

Fig. 3: Residual error in velocity, temperature, and concentration functions at different $'n'$

Figures 3(a)-3(c) display the residual error in velocity, temperature, and concentration functions at varied values of the nonlinear parameter n. It once again validates the reliability and accuracy of the spectral method.

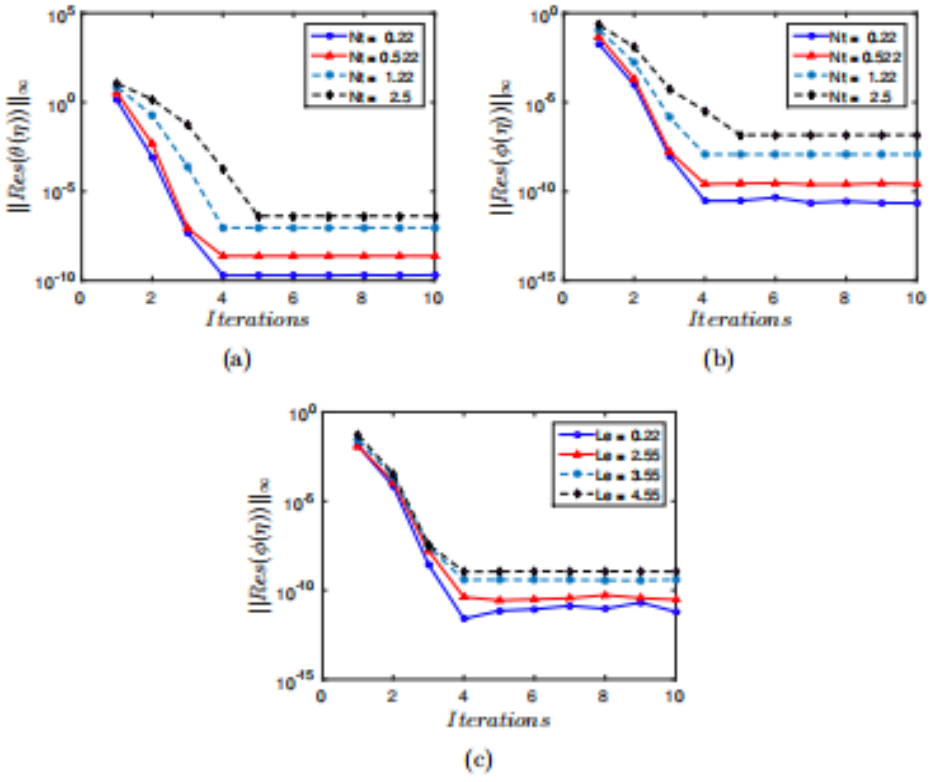

Fig. 4: Residual error in temperature and concentration functions at different Nt and Le

The residual error in temperature and concentration functions is plotted in figures 4(a),(b) to demonstrate the impact of thermophoresis parameter. Figure 4(c) displays the residual error in concentration function for different Lewis parameter. It may be noticed from figures 4(a)-4(c) that stability has been achieved and convergence to the order of 10^{-10} is reached in four iterations.

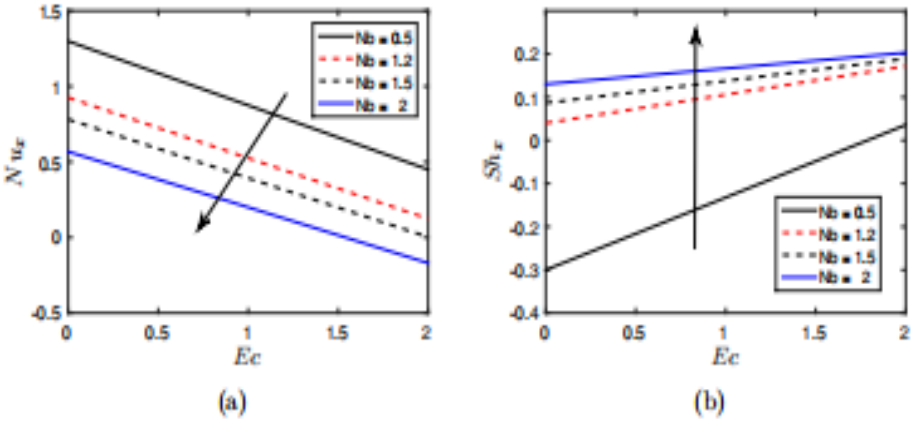

Fig. 5: Local Nusselt and Sherwood numbers at different Nb

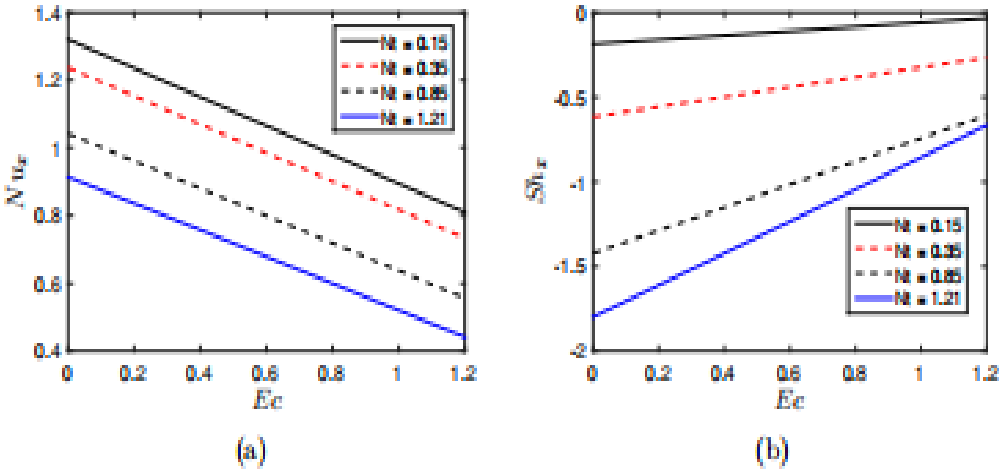

Fig. 6: Local Nusselt and Sherwood numbers at different Nt

To justify the physical consequences of the flow problem presented here, detailed investigation is performed for varied values of the flow parameters of interest. The outcome is displayed graphically and analyzed. Figures 5(a) and 5(b) display the local Nusselt and Sherwood numbers with Eckert number Ec at different Brownian motion parameter Nb. One may observe that with the rise in Eckert number, Nusselt number shows a decreasing trend for a specified Nb. However, Sherwood number manifests a positive correlation with Eckert number. It can be as well noted that with an enhancement in Nb, Sherwood number also increases, whereas Nusselt number is found to decline. Figures 6(a), 6(b) portray the behaviour of Nusselt and Sherwood numbers with thermophoresis parameter Nt. Both Nu_x and Sh_x show a negative correlation with Nt. Basically, this implies that the rate of heat transfer diminishes as the Brownian motion as well as thermophoresis parameters increase. On the contrary, the rate of mass transfer escalates with Brownian motion parameter, but diminishes with rise in thermophoresis parameter.

Figure 7 illustrates the variation of entropy with Brinkman number Br. Increment of Br causes an enhancement of the entropy number near the wall. Thermal radiation may be responsible for the heat generation in the system close to the surface by transporting the heat through molecular conductivity. Figure 8 displays the influence of Brinkman number on Bejan number. In this case, a decreasing effect is observed on Bejan number with increment in Br. Figure 9 presents the changes in

entropy generation number with different temperature ratio parameters. With the increment in magnetic parameter, entropy generation number is also increased. We may note that entropy generation number increases comparatively more when Reynolds number Re rises. The effect of increment of parameter χ on Bejan number is displayed in figure 10.

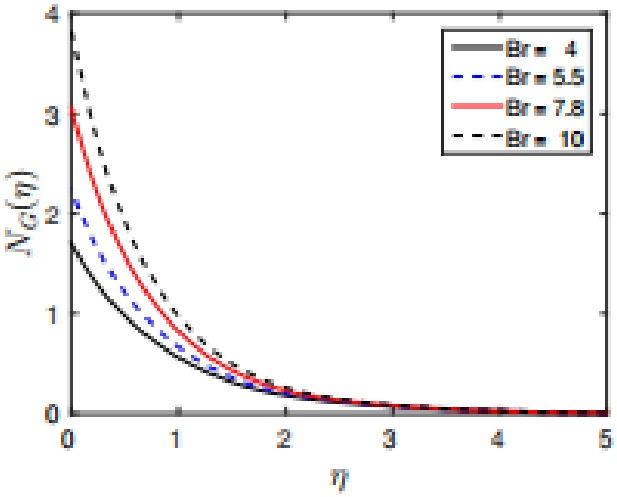

Fig. 7: Entropy generation number at different Brinkman number

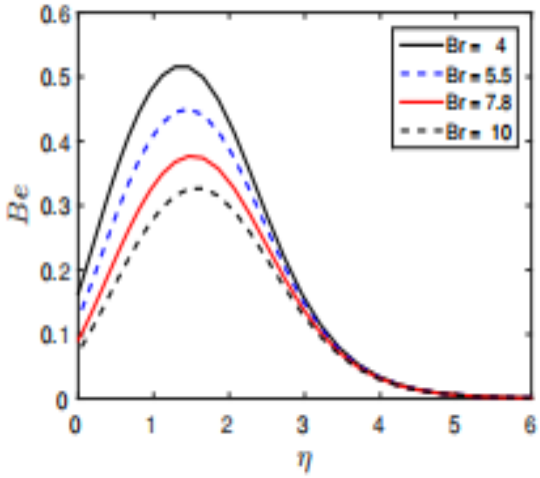

Fig. 8: Bejan number at different Brinkman number

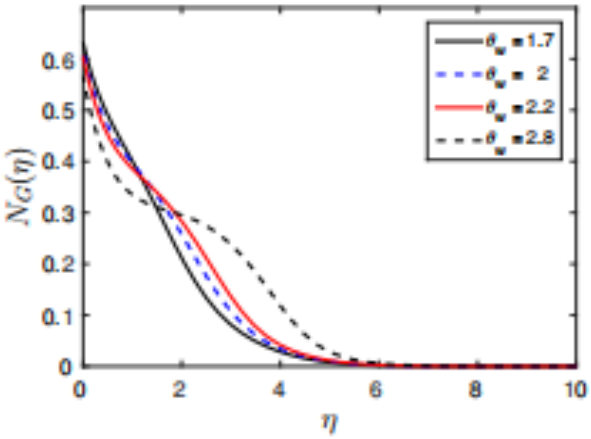

Fig. 9: Entropy generation number with different temperature ratio parameter

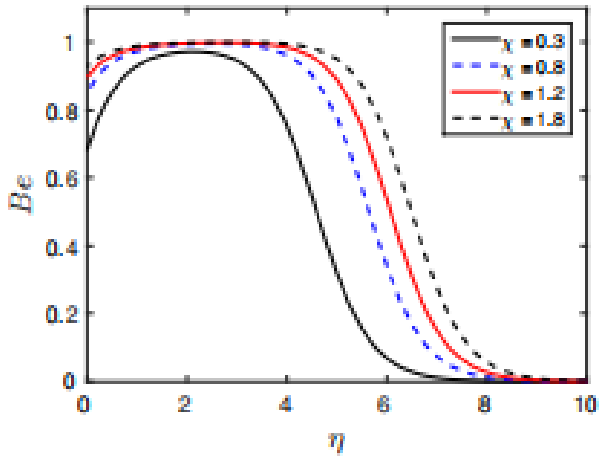

Fig 10: Bejan number at varied values of the parameter (χ)

8 Concluding Remarks

A steady MHD nanofluid flow across non-linear stretching boundary layer with viscous dissipation and thermal radiation is scrutinized thoroughly for different parameters of interest. The constitutive equations have been non-dimensionalised using standard similarity transformation and thereafter solved using the spectral quasil-linearisation method. Entropy generation analysis is also performed for the flow model. Error analysis is conducted and analysed carefully.

This kind of research has extensive applications in various technological, scientific, industrial, and biomedical domains. The important highlights of this study are as follows:

(i) The error in calculation of velocity, temperature, and concentration profiles diminishes to the order of 10^{-8} or less in just five iterations. This affirms the convergence as well as stability of the numerical scheme presented in this work.

(ii) The heat transfer rate exhibits a negative correspondence with theromophoresis as well as Brownian motion parameters. It may be noted that increment in the thermophoresis parameter diminishes the heat transfer rate due to the movement of the nanoparticles away from hotter regions. Further, an increment in the Brownian motion parameter implies an enhancement in the random movement of nanoparticles due to collisions with molecules of the base fluid. This leads to thining of concentration in the boundary layer and it eventually reduces the overall heat transfer.

(iii) The rate of mass transfer rate gets escalated with the increase of Brownian motion parameter. Elevation of the Brownian motion parameter implies that the particles are moving more actively. This leads to a faster mixing and hence enhances the rate of mass transfer. However, a decreasing tendency may be noted with increment of thermophoresis parameter. In the context of mass transfer, a rise in the thermophoresis parameter indicates that the particles are more sensitive to temperature differences. This leads to the movement of the particles away from hotter regions, thus diminishing the overall mass transfer rate.

References

1. A. Patra, M. K. Nayak, A. Misra, Effects of Non-uniform Suction, Heat Generation/Absorption and Chemical Reaction with Activation Energy on MHD Falkner - Skan Flow of Tangent Hyperbolic Nanofluid over a Stretching/ Shrinking Edge. Journal of Applied and Computational Mechanics, **6(3)**, 640 – 652 (2020).
2. M. I. Afridi, M. Qasim, I. Khan, Entropy Generation Minimization in MHD Boundary Layer Flow over a Slendering Stretching Sheet in the Presence of Frictional and Joule Heating. Journal of the Korean Physical Society, **73**, 1303 – 1309 (2018).
3. Z. Shah, P. Kumam, W. Deebani, Radiative MHD Casson Nanofluid Flow with Activation energy and chemical reaction over past nonlinearly stretching surface through Entropy generation. Scientific Reports, **10**, 4402 (2020).
4. G. Sandhya, G. Sarojamma, P. V. Satya Narayana, B. Venkateswarlu, Buoyancy forces and activation energy on the MHD radiative flow over an exponentially stretching sheet with second-order slip. Heat Transfer, **50(1),** 784 – 800 (2021).
5. E. R. El-Zahar, A. M. Rashad, L. F. Seddek, Impacts of Viscous Dissipation and Brownian motion on Jeffrey Nanofluid Flow over an Unsteady Stretching Surface with Thermophoresis. Symmetry, **12(9),** 1450 (2020).
6. M. A. Qureshi, Numerical Simulation of Heat Transfer Flow Subject to MHD of Williamson Nanofluid with Thermal Radiation. Symmetry, **13(1),** 10 (2020).
7. S. Alqaed, J. Mustafa, M. Sharifpur, Numerical investigation and optimization of natural convection and entropy generation of alumina/H_2O nanofluid in a rectangular cavity in the presence of a magnetic field with artificial neural networks. Engineering Analysis with Boundary Elements, **140**, 507 – 518 (2022).
8. Z. U. Din, A. Ali, A., M. De la Sen, G. Zaman, Entropy generation from convective - radiative moving exponential porous fins with variable thermal conductivity and heat generations. Scientific Reports, **12**, 1791 (2022).
9. Z. U. Din, A. Ali, A., G. Zaman, Entropy generation in moving exponential porous fins with natural convection, radiation and internal heat generation. Archive of Applied Mechanics, **92(3),** 933 – 944 (2022).
10. H. K. Hamzah, F. H. Ali, M. Hatami, MHD mixed convection and entropy generation of CNT-water nanofluid in a wavy lid- driven porous enclosure at different boundary conditions. Scientific Reports, **12**, 2881 (2022).
11. A. Shahsavar, P. Farhadi, C. Yildiz, M. Moradi, M. Arici, Evaluation of entropy generation characteristics of boehmite - alumina nanofluid with different shapes of nanoparticles in a helical heat sink. International Journal of Mechanical Sciences, **225**, 107338 (2022).
12. M. Mahboobtosi, Kh. Hosseinzadeh, D.D. Ganji, Entropy generation analysis and hydrothermal optimization of ternary hybrid nanofluid flow suspended in polymer over curved stretching surface. International Journal of Thermofluids, **20**, 100507 (2020). https://doi.org/10.1016/j.ijft.2023.100507
13. R. M. Zulqarnain, .M. Nadeem, I. Siddique, et al. Impacts of entropy generation in second-grade fuzzy hybrid nanofluids on exponentially permeable stretching/shrinking surface. Scientific Reports, **13**, 22132 (2023). https://doi.org/10.1038/s41598-023-48142-0
14. K. Rafique, Z. Mahmood, A. Adnan, U. Khan, T. Muhammad, M. Abd, S. A. Bajri, H. Abd, Numerical investigation of entropy generation of Joule heating in non-axisymmetric flow of hybrid nanofluid towards stretching surface. Journal of Computational Design and Engineering, **11(2),** 146-160 (2024). https://doi.org/10.1093/jcde/qwae029
15. G. Ramasekhar, M. Jawad, S. Jakeer, S. Reddy, R. Reddy, Entropy Generation for Novel Trend of Biomedical Aspects on Magnetohydrodynamics Hybrid Nanofluid Flow Through a Stretching Cylinder. J. Nanofluids, **13**, 1021–1029 (2024).
16. R. D. Murugan, N. Sivakumar, N. Tarakaramu, et al. Entropy generation on MHD motion of hybrid nanofluid with porous medium in presence of thermo-radiation and ohmic viscous dissipation. Discov Appl Sci, **6**, 199 (2024). https://doi.org/10.1007/s42452-024-05866-6
17. M. Rafiq, M. Shazadi, G. I. H. Aslam, N. B. Khedher, S. M. Tag-Eldin, K. Guedri, Entropy generation analysis of hybrid nanofluid through flexible tube with convective conditions. International Journal of Modern Physics B, **38**, **(16)** 2450208 (2024). https://doi.org/10.1142/S0217979224502084

18. S.S. Samantaray, A. Misra, S. Shaw, M. K. Nayak, S. Nazari, I. Boukhris, A. J. Chamkha, Recent advances on entropy analysis of composite nanofluids-A critical review. Results in Engineering, **22,** 101980 (2024). https://doi.org/10.1016/j.rineng.2024.101980
19. M. Sheikholeslami, D. D. Ganji, M. Gorji-Bandpay, S. Soleimani, Magnetic field effect on nanofluid flow and heat transfer using KKL model. Journal of the Taiwan Institute of Chemical Engineers, **45(3),** 795-807 (2014).
20. H. Heidary, R. Hosseini, M. Pirmohammadi, M. J. Kermani, Numerical study of magnetic field effect on nano-fluid forced convection in a channel. Journal of Magnetism and Magnetic Materials, **374**, 11-17 (2015).
21. M. Sheikholeslami, M., D. D. Ganji, M. M. Rashidi, Magnetic field effect on unsteady nanofluid flow and heat transfer using Buongiorno model. Journal of Magnetism and Magnetic Materials, **416**, 164-173 (2016).
22. M. Imran, U. Farooq, T. Muhammad, S. U. Khan, H. Waqas, Bioconvection transport of Carreau nanofluid with magnetic dipole and nonlinear thermal radiation. Case Studies in Thermal Engineering, **26**, 101129 (2021).
23. B. Ali, S. Hussain, S. Abdal, M. M. Mehdi, Impact of Stefan blowing on thermal radiation and Cattaneo-Christov characteristics for nanofluid flow containing microorganisms with ablation/accretion of leading edge: FEM approach.The European Physical Journal Plus,**135**, 821 (2020).
24. H. Waqas, M. Imran, T. Muhammad, S. M. Sait, R. Ellahi, On bio-convection thermal radiation in Darcy-Forchheimer flow of nanofluid with gyrotactic motile microorganism under Wu's slip over-stretching cylinder/plate. International Journal of Numerical Methods for Heat and Fluid Flow, **31(5),** 1520-1546 (2020).
25. H. Waqas, M. Imran, T. Muhammad, S. M. Sait, R. Ellahi, Numerical investigation on bioconvection flow of Oldroyd-B nanofluid with nonlinear thermal radiation and motile microorganisms over rotating disk. Journal of Thermal Analysis and Calorimetry, **145(2),** 523-539 (2021).
26. M. I. Khan, H. Waqas, S. U. Khan, M. Imran, Y-M. Chu, A. Abbasi, S. Kadry, Slip flow of micropolar nanofluid over a porous rotating disk with motile microorganisms, nonlinear thermal radiation and activation energy. International Communications in Heat and Mass Transfer, **122**, 105161 (2021).
27. K. Al-Khaled, S. U. Khan, I. KhanChemically reactive bioconvection flow of tangent hyperbolic nanoliquid with gyrotactic microorganisms and nonlinear thermal radiation. Heliyon, **6(1),** e03117, (2020).
28. Usman, W. A. Khan, N. Uddin, T. Muhammad, Heat and mass transport in an electrically conducting nanofluid flow over two-dimensional geometries. Heliyon, **9(8),** e18377 (2023). https://doi.org/10.1016/j.heliyon.2023.e18377
29. M. Arshad, F. M. Alharbi, A. Hassan, Q. Haider, A. Alhushaybari, S. M. Eldin, Z. A. L. Ahmad, A. M. Galal, Effect of inclined magnetic field on radiative heat and mass transfer in chemically reactive hybrid nanofluid flow due to dual stretching. Scientific Reports, **13(1**), 1-16 (2023). https://doi.org/10.1038/s41598-023-34871-9
30. F. Xu, Y. Cao, H. Gong, J. Li, Y. Xu, L. Shi, Mass Transport and Energy Conversion of Magnetic Nanofluids from Nanoparticles' Movement and Liquid Manipulation. Processes, **12(5),** 955 (2024). https://doi.org/10.3390/pr12050955